machines

MDPI

Article

EKF- and ESKF-Based GNSS/INS Integrated Navigation Under the Interaction Multi-Filter Framework

Shichao Zhang, Zi Yang * and Chenxiao Cai

School of Automation, Nanjing University of Science and Technology, 200 Xiaolingwei Street, Xuanwu District, Nanjing 210094, China; 123110223333@njust.edu.cn (S.Z.); ccx5281@njust.edu.cn (C.C.)
* Correspondence: yangzi@njust.edu.cn

Abstract

In multirotor unmanned aerial vehicle (UAV) GNSS/INS integrated navigation systems, a single filter such as the extended Kalman filter (EKF) or the error-state extended Kalman filter (ESKF) is commonly adopted. However, both methods have inherent performance limitations. The EKF suffers from significant linearization errors in highly nonlinear flight scenarios, leading to degraded estimation accuracy. Although ESKF achieves higher precision during steady flight, its model assumptions may no longer strictly hold during aggressive maneuvers, causing performance degradation in complex flight missions. To address the limitations of using a single filter, this study proposes a dynamic filter selection strategy under the interaction multi-filter (IMF) framework. The approach builds on the interactive multiple model (IMM) method and establishes a cooperative mechanism between EKF and ESKF. By computing the filter likelihoods at each time step and updating the probability switching matrix, the framework adaptively selects the optimal filter based on the current flight conditions. Simulation results demonstrate that the proposed IMF-based strategy effectively avoids the performance bottlenecks of individual filters. In highly nonlinear environments, it reduces linearization errors and suppresses divergence trends; compared with traditional ESKF, the proposed algorithm 3D RMSE is reduced by 57.2%, compared with the adaptive robust EKF (AREKF), the proposed approach reduces positioning errors by up to 21.3%. The results confirm that IMF-based adaptive switching between EKF and ESKF yields a robust, high-precision solution for UAV navigation in complex operational scenarios.

Keywords: GNSS/INS integration; EKF; ESKF; interaction multi-filter (IMF); UAV navigation; nonlinear estimation

Check for updates

Academic Editor: Ahmed Abu-Siada

Received: 11 December 2025
Revised: 9 February 2026
Accepted: 10 February 2026
Published: 12 February 2026

Copyright: © 2026 by the authors. Licensee MDPI, Basel, Switzerland. This article is an open access article distributed under the terms and conditions of the Creative Commons Attribution (CC BY) license.

1. Introduction

With the rapid development of the low-altitude economy, multirotor unmanned aerial vehicles (UAVs) have become a key technological tool due to their strong vertical takeoff and landing capability, high maneuverability, controllable cost, and ease of operation [1,2]. They have been widely applied across sectors of the national economy, thereby improving productivity, reducing operational risks, and expanding their application boundaries [3]. Currently, multirotor UAVs have been widely deployed in various applications, including agricultural plant protection, logistics and delivery, emergency rescue, construction surveying, aerial cinematography, and military reconnaissance [4,5].

For navigation and positioning requirements of multirotor UAVs, the global navigation satellite system (GNSS) and the inertial navigation system (INS) are the two most widely

used technical solutions [6,7]. GNSS provides high absolute positioning accuracy and long-term stability, but it is highly dependent on external environmental conditions. Its signals are easily affected by obstructions (e.g., urban canyons), electromagnetic interference, and multipath effects, leading to significant degradation of positioning accuracy in complex scenarios [8–10]. INS, on the other hand, uses data from the inertial measurement unit (IMU) to provide high-frequency, continuous estimates of position, velocity, and attitude. It offers autonomy, short-term accuracy, and independence from external signals. However, due to bias drift, scale-factor errors, and random noise of accelerometers and gyroscopes, INS errors grow exponentially over time, rendering it insufficient for long-term navigation when used alone [11–13].

In practical engineering applications, relying solely on GNSS or INS cannot satisfy the dual demands of high precision and strong robustness in complex UAV navigation environments [14]. GNSS/INS integrated navigation combines the long-term accuracy of GNSS with the short-term stability of INS, thereby compensating for their respective shortcomings and enhancing the overall performance of the navigation system [15]. This integrated approach has become a core enabling technology in UAVs, autonomous driving, precision guidance, and mobile robotics [16]. However, the expanding operational domains of UAVs have imposed increasingly stringent requirements on the accuracy and robustness of GNSS/INS integrated navigation [17]. Designing filtering algorithms that can fully exploit the performance potential of GNSS/INS in complex dynamic environments, while simultaneously achieving high stability, precision, and real-time capability, remains a critical challenge in this field.

Among various GNSS/INS filtering methods, the extended Kalman filter (EKF) is the earliest nonlinear filtering technique implemented in engineering practice [18,19]. Its core idea is to approximate a nonlinear system by linearizing it through a first-order Taylor expansion, followed by classical Kalman filter recursion. The EKF can achieve satisfactory state-estimation accuracy in low- or mildly nonlinear scenarios and was therefore widely used in early integrated navigation systems [20]. When the system becomes highly nonlinear or the state covariance becomes large, the linearization error increases substantially, reducing accuracy and stability and potentially leading to divergence [21].

To mitigate the limitations of the EKF, the error-state extended Kalman filter (ESKF) has become a focus of research in recent years [22]. Unlike EKF, ESKF does not directly linearize the full state of the system. Instead, it constructs an error-state model by decomposing the system into a nominal state and an error state, linearizing only the error component. This approach substantially improves numerical stability and estimation accuracy [23]. ESKF has demonstrated good practical performance in scenarios such as steady UAV flight and mobile robot localization. At the same time, during aggressive UAV maneuvers (e.g., rapid turns or accelerations), the discrepancy between the assumed error model and the actual motion increases, leading to significant estimation biases and performance degradation [24]. Hence, although considerable progress has been made in the theoretical analysis and application of EKF and ESKF, both remain inherently limited in complex environments—the linearization of full state in EKF gives rise to non-negligible errors, and ESKF underperforms in high-dynamic flight. Existing solutions lack flexibility and fail to ensure accuracy and stability across diverse flight conditions simultaneously.

To further enhance the robustness of integrated navigation filtering, multi-model fusion frameworks have been introduced. The most representative approach is the interacting multiple model (IMM) method [25]. The IMM algorithm constitutes a classical framework for multiple model adaptive filtering (MMAF), originally proposed by Blom and Bar-Shalom in 1988 for maneuvering target state estimation in target tracking applications. IMM constructs multiple parallel sub-models to match different motion modalities, updat-

ing each model through interaction and probabilistic weighting to achieve high-precision state estimation in multimodal switching systems [26]. Extending IMM, the interaction multi-filter (IMF) framework was proposed. Unlike traditional IMM, which only switches among models of the same filter type, IMF enables dynamic selection and switching among different filters—specifically EKF and ESKF.

In this context, this paper proposes a GNSS/INS integrated navigation algorithm based on the IMF framework. The proposed framework operates EKF and ESKF in parallel and adaptively switches between them according to the UAV's flight dynamics, prioritizing ESKF during steady flight for high-precision estimation and favoring EKF under highly nonlinear or aggressive maneuvering conditions to maintain filter stability.

The main contributions of this paper can be summarized as follows:

First, an IMF-based integrated navigation framework is proposed to enable cooperative operation and probabilistic switching between EKF and ESKF, effectively balancing navigation accuracy and robustness across different flight regimes.

Second, an adaptive model probability update mechanism is developed by integrating residual-based likelihood evaluation with a maneuver-sensitive preference function. By jointly exploiting measurement residuals and flight dynamics information, the proposed mechanism effectively smooths filter transitions and alleviates the switching instability and lag commonly observed in purely residual-based approaches.

Third, comparative simulations demonstrate that the proposed strategy significantly outperforms standalone filtering methods in terms of positioning accuracy and robustness. Furthermore, compared to the adaptive robust EKF (AREKF), the proposed IMF-based approach exhibits superior resilience to model mismatch and maneuver-induced disturbances, effectively mitigating error accumulation under highly nonlinear flight conditions.

2. Mathematical Models

2.1. IMU Kinematics and Error Models

An inertial measurement unit (IMU) typically consists of a three-axis accelerometer and a three-axis gyroscope, whose outputs are used to derive the vehicle's current attitude, velocity, and position. The fundamental IMU measurement equations can be expressed as

$$\tilde{f} = f + b_a + n_a \tag{1}$$

$$\tilde{\omega} = \omega + b_g + n_g \tag{2}$$

where $\tilde{f}$ and $\tilde{\omega}$ are the measured accelerometer and gyroscope outputs, f and ω are the true values, b_a and b_g represent accelerometer and gyroscope biases, and n_a and n_g denote measurement noise. The recursive inertial navigation process includes attitude, velocity, and position updates, as follows:

(1) Attitude update:

$$\dot{C}_b^n = C_b^n[\tilde{\omega} - b_g - n_g]_\times - [\omega_{in}^n]_\times C_b^n \tag{3}$$

where $[\cdot]_\times$ denotes the skew-symmetric operator and ω_{in}^n denotes angular velocity of the navigation frame relative to the inertial frame used to update roll, pitch, and yaw.

(2) Velocity update:

$$\dot{v}_n = C_b^n(\tilde{f} - b_a - n_a) + g_n \tag{4}$$

where v_n is the velocity in the navigation frame and g_n is the gravity vector.

(3) Position update:

$$\dot{p}_n = v_n \tag{5}$$

These equations describe the ideal inertial navigation process. However, due to bias and scale factor errors, INS position and attitude errors grow rapidly over time. A common bias model is the first-order Markov process:

$$\dot{b}_a = -\frac{1}{\tau_a} b_a + w_a \, , \dot{b}_g = -\frac{1}{\tau_g} b_g + w_g \tag{6}$$

where τ_a and τ_g are the time constants, and w_a and w_g is white noise. As a result, IMU outputs can be regarded as the combination of true values, stochastic drift, and noise—this constitutes the primary source of errors addressed by the filtering algorithm.

2.2. GNSS Measurement Model

GNSS observations provide position and velocity measurements in the NED frame. For simplicity, we model GNSS errors as Gaussian. The position observation equation is given by

$$z_p = p^n + n_p \tag{7}$$

where p_n is the true position and n_p is measurement noise. The velocity observation equation is:

$$z_v = v^n + n_v \tag{8}$$

where v^n is the true velocity and n_v is noise. These measurements serve as reference inputs for updating the filter.

In practice, GNSS measurement errors arise from satellite clock and orbit errors, ionospheric and tropospheric delays, multipath effects, and receiver thermal noise. Ionospheric and tropospheric delays can be modeled and compensated. Multipath effects and sensor receiver thermal noise are typically approximated as Gaussian white noise for filtering purposes. Although this assumption is not entirely accurate, it is effective in integrated navigation systems.

2.3. System State and Observation Equations

To achieve INS/GNSS fusion within a filtering framework, the system state vector must be defined. This work adopts the following state representation:

$$x = \left[\delta p^n \; \delta v^n \; \delta\theta \; b_a \; b_g\right]^T \tag{9}$$

where δp^n is the position error, δv^n is the velocity error, $\delta\theta$ is the attitude error, and b_a and b_g are accelerometer and gyroscope biases, respectively. The state equation is:

$$\dot{x} = Fx + Gw \tag{10}$$

where F is the state transition matrix, w is the process noise, and G is the noise-driving matrix, describing INS error propagation. The observation equation is built upon the difference between GNSS measurements and INS estimates:

$$z = \begin{bmatrix} z_p - \hat{p}^n \\ z_v - \hat{v}^n \end{bmatrix} = Hx + n \tag{11}$$

where H is the observation matrix and n is the measurement noise. These models provide a unified mathematical foundation for EKF, ESKF, and the IMF framework. EKF directly linearizes the full state vector, while ESKF filters the error state to preserve numerical stability. The IMF framework further enables the parallel execution of both filters and the dynamic selection of the optimal one.

This section establishes the mathematical basis of GNSS/INS integrated navigation, including IMU kinematics and error modeling, GNSS measurements, and system state and observation equations. These models support the development of the EKF, ESKF, and IMF framework described in the following section.

3. Integrated Navigation Algorithms

3.1. Extended Kalman Filter Models

The extended Kalman filter is one of the most widely used nonlinear filtering methods in GNSS/INS integrated navigation. Its core concept is to linearize the nonlinear system via a first-order Taylor expansion, ignoring higher-order terms, and then perform recursive estimation using the classical Kalman filter. Assume the system state and observation equations are:

$$x_k = f(x_{k-1}, u_{k-1}) + w_{k-1} \tag{12}$$

$$z_k = h(x_k) + v_k \tag{13}$$

where $f(\cdot)$ is the nonlinear state transition function that propagates the previous state x_{k-1} to the current state x_k using control input u_{k-1}, $h(\cdot)$ is the nonlinear observation function that maps the current state x_k to the expected sensor measurement z_k, and w_{k-1} and v_k are zero-mean white noise processes representing process noise and measurement noise, respectively. The EKF procedure consists of two main steps:

(1) Prediction step

Use the previous state and covariance to predict the current state:

$$\hat{x}_{k|k-1} = f\left(\hat{x}_{k-1|k-1}, u_{k-1}\right) \tag{14}$$

$$P_{k|k-1} = F_{k-1} P_{k-1|k-1} F_{k-1}^T + Q_{k-1} \tag{15}$$

where F_{k-1} is the Jacobian of $f(\cdot)$ with respect to the state. The matrix Q_{k-1} denotes the discrete-time process noise covariance matrix. It is obtained by discretizing the continuous-time process noise model under the assumption of a short sampling interval. In this work, Q_{k-1} is approximated using a first-order discretization as

$$Q_{k-1} \approx G Q_c G^T \delta t \tag{16}$$

where G is the continuous-time noise mapping matrix, Q_c is the continuous-time power spectral density matrix of the system noise, and Δt is the sampling interval. The matrix Q_c is constructed based on the stochastic error characteristics of the IMU, including velocity random walk, angle random walk, and the driving noise variances associated with the first-order Gauss–Markov models of sensor biases.

(2) Update step

GNSS measurements are used to correct the predicted state:

$$K_k = P_{k|k-1} H_k^T \left(H_k P_{k|k-1} H_k^T + R_k\right)^{-1} \tag{17}$$

$$\hat{x}_{k|k} = \hat{x}_{k|k-1} + K_k \left(z_k - h\left(\hat{x}_{k|k-1}\right)\right) \tag{18}$$

$$P_{k|k} = (I - K_k H_k) P_{k|k-1} \tag{19}$$

The EKF is easy to implement, has a moderate computational cost, and performs well in weakly nonlinear scenarios. However, in highly nonlinear or rapidly varying conditions, linearization errors can lead to significant bias or even filter divergence.

3.2. Error-State Kalman Filter Models

The error-state Kalman filter enhances numerical stability and estimation accuracy by modeling and updating the error state, rather than linearizing the full system state. The system state is decomposed into a nominal state and an error state:

$$x = \bar{x} \oplus \delta x \tag{20}$$

where $\bar{x}$ is the nominal state obtained by integrating inertial equations, and δx is the error state defined in additive or multiplicative form (e.g., quaternions for attitude). The error state is propagated according to the error dynamics:

$$\dot{\delta x} = F\delta x + Gw \tag{21}$$

where F is the Jacobian of the error dynamics with respect to the error state, G is the noise mapping matrix, and w denotes zero-mean Gaussian white process noise associated with IMU measurement errors.

The continuous-time error dynamics are discretized with sampling interval Δt. In the prediction step, since the error mean is maintained at zero, only the covariance matrix is propagated:

$$P_{k|k-1} = F_{k-1}P_{k-1|k-1}F_{k-1}^T + Q_{k-1} \tag{22}$$

where $P_{k|k-1}$ denotes the predicted error-state covariance, and Q_{k-1} is the discrete-time process noise covariance matrix. When GNSS updates are available, the Kalman gain K_k is computed:

$$K_k = P_{k|k-1}H_k^T(H_kP_{k|k-1}H_k^T + R_k)^{-1} \tag{23}$$

where H_k is the Jacobian of the measurement model with respect to the error state, and R_k denotes the measurement noise covariance matrix. Subsequently, the error state estimate and covariance are updated:

$$\delta x_{k|k} = K_k(z_k - h(\bar{x}_{k|k-1})) \tag{24}$$

$$P_{k|k} = (I - K_kH_k)P_{k|k-1} \tag{25}$$

where z_k represents the measurement vector and $h(\cdot)$ is the nonlinear measurement function evaluated at the nominal state. Finally, the estimated error is injected into the nominal state. For attitude, this is performed via quaternion multiplication:

$$q_{new} = \delta q \otimes \bar{q} \tag{26}$$

where δq denotes the small-angle error quaternion and $\otimes$ represents quaternion multiplication. After the injection, the error state vector δx is reset to zero to maintain the validity of the linearization on the manifold.

Compared to the EKF, the ESKF offers higher numerical stability and better handling of strongly nonlinear states, such as attitude, and is widely applied in the aerospace, UAV, and robotics domains. However, under highly dynamic maneuvers, the assumed error-state model may no longer accurately represent the true system behavior, which can lead to performance degradation and, in some cases, inferior performance compared with the EKF.

3.3. Dynamic Filter Selection Under the IMF Framework

The interaction multi-filter framework is inspired by the interacting multiple model method. IMM is an advanced algorithm used primarily for target tracking and state estimation in dynamic systems, where the behavior of the tracked object can change unpredictably

over time. Conventional IMM employs homogeneous sub-model sets that modify the state transition matrix within the EKF framework, essentially preserving a single-filter architecture that cannot simultaneously address the dual objectives of efficiency and robustness. Moreover, model probability updates in classical IMM rely primarily on observation likelihoods, which provide a direct and theoretically grounded measure of model–measurement consistency. However, likelihoods alone can be highly sensitive to transient measurement noise and large residuals during aggressive maneuvers, causing frequent or oscillatory mode switches. To improve robustness and to account for flight dynamics, we therefore augment the residual-based likelihood with a maneuver-sensitive prior, so that likelihood information and dynamics-aware prior jointly determine model probabilities.

The core idea of IMF is to run multiple filters in parallel and dynamically update their weights based on observation likelihoods, enabling adaptive selection of the optimal filter under different operating conditions. Unlike traditional IMM, which switches among models of the same filter type, the IMF framework supports switching between distinct filtering methods such as EKF and ESKF, allowing their complementary advantages to be exploited under varying flight dynamics.

To implement the IMF process, the EKF and ESKF operate in parallel at each time step, generating state estimates and covariance matrices. Filter weighting and selection is based on the likelihood of residuals. For each filter, the residual is:

$$r_k^{(i)} = z_k - h\left(\hat{x}_{k|k-1}^{(i)}\right) \tag{27}$$

Assuming zero-mean Gaussian measurement noise, the residual likelihood is computed as

$$\Lambda^{(i)} = \frac{1}{\sqrt{(2\pi)^m |S^{(i)}|}} \exp\left(-\frac{1}{2} r_k^{(i)T} S^{(i)-1} r_k^{(i)}\right) \tag{28}$$

where m is the measurement dimension and $S^{(i)}$ is the residual covariance matrix, given by

$$S^{(i)} = H^{(i)} P_{k|k-1}^{(i)} H^{(i)T} + R \tag{29}$$

For EKF and ESKF, the measurement Jacobians and covariance matrices are defined in their respective state spaces, and the likelihood is computed in a consistent measurement residual space.

The filter linearization error is strongly correlated with angular acceleration and jerk, which in turn correspond to the derivatives of the angular and velocity increments measured by the IMU. Accordingly, a maneuver intensity index is defined as

$$M_k = \alpha \cdot \frac{\|\dot{\omega}_k\|}{s_\omega} + \beta \cdot \frac{\|\dot{a}_k\|}{s_a} \tag{30}$$

where $\dot{\omega}_k$ and $\dot{a}_k$ represent the time derivatives of gyroscope and accelerometer outputs. The derivatives are approximated using finite differences of discrete IMU measurements, followed by a smoothing operation to suppress noise amplification; α and β denote weighting factor, default 0.5; s_ω and s_a are normalization factors.

The distinction between steady flight and aggressive maneuvering is not defined by fixed absolute thresholds. Instead, it is determined relative to the UAV platform capabilities and the statistical characteristics of the actual flight data. This relative definition ensures adaptability to different UAV platforms and mission profiles and avoids the use of empirically fixed thresholds with limited generality.

$$\dot{\omega}_k = \frac{\omega_k - \omega_{k-1}}{\Delta t} \dot{a}_k = \frac{a_k - a_{k-1}}{\Delta t} \tag{31}$$

where Δt denotes the discrete sampling interval of the IMU. In our experiments, Δt corresponds to the IMU sampling interval and equals 1/200 s; dataset-specific sampling settings are reported in Section 4. The derivatives are smoothed using a first-order exponential filter to suppress noise amplification.

$$x_k^m = \gamma x_{k-1}^{sm} + (1 - \gamma) x_k \tag{32}$$

where γ is 0.95. To achieve balanced contributions, the smoothed angular acceleration and jerk are normalized using scaling factors derived from their respective 95th percentiles across the dataset. Employing the 95th percentile as the scaling basis avoids undue influence from extreme outliers while preserving the characteristic magnitude of intense but plausible maneuvers.

$$s_\omega = percentile_{95}(\|\dot{\omega}_k^{sm}\|) \tag{33}$$

$$s_a = percentile_{95}(\|\dot{a}_k^{sm}\|) \tag{34}$$

The flight state thresholds are defined based on the maneuver detection index M_k, which quantifies the intensity of the UAV's dynamic motion. These thresholds are used to classify the UAV's flight state according to the maneuver intensity. The distinction between steady flight and aggressive maneuvering is defined relative to the platform capabilities and the statistical characteristics of the flight data. In this study, when M_k exceeds 0.3, the UAV is considered to have entered a maneuvering state. A value of M_k greater than 0.6 indicates that the UAV is in an aggressive maneuvering state.

The filter preference function is defined based on maneuver intensity to dynamically adjust the transition probabilities. The filter preference functions of ESKF and EKF are chosen to be smooth, monotonic, and bounded in (0, 1).

$$f_{ESKF}(M_k) = \exp(-\lambda M_k) \tag{35}$$

$$f_{EKF}(M_k) = 1 - \exp(-\lambda M_k) \tag{36}$$

where $f_i(M_k)$ denotes the maneuver-dependent preference function associated with the ith filter; f_{ESKF} decreases and f_{EKF} increases with maneuver intensity. The exponential form is adopted for its simplicity, continuous differentiability, and tunable sensitivity via the scalar λ. This design reflects the fact that EKF does not rely on small-error assumptions inherent in error-state formulations, making it more tolerant to severe nonlinearities during aggressive maneuvers.

The transition from steady cruising to aggressive maneuvering in UAVs is typically abrupt and non-stationary. During such phases, the estimation error may not immediately increase, while the mismatch between the assumed error model and the actual motion dynamics grows rapidly. To address this issue, the IMF framework dynamically adjusts the weight allocation between EKF and ESKF once the maneuver intensity index M_k exceeds a predefined threshold. This mechanism enables smooth filter preference adaptation and mitigates performance degradation and switching transients caused by delayed responses.

In the proposed framework, filter probabilities are jointly determined by the measurement residual statistics and the maneuver intensity. For each filter, an unnormalized weighting factor is first computed as the product of the residual likelihood and the maneuver-based preference function. The normalized filter probability is then obtained as

$$\mu_k^{(i)} = \frac{\Lambda^{(i)} f_i(M_k)}{\sum_{l=1}^{2} \Lambda^{(l)} f_l(M_k)} \tag{37}$$

where $\mu_k^{(i)}$ denotes the probability associated with the ith filter, $\Lambda^{(i)}$ is the residual likelihood, and $f_i(M_k)$ represents the maneuver-dependent preference function.

Similarly, the transition probabilities between filters are updated based on the prior transition matrix, maneuver intensity, and residual likelihood. The unnormalized transition probability is defined as

$$\tilde{p}_{ij}(k) = p_{ij,0} \cdot f_j(M_k) \cdot \Lambda^{(j)} \tag{38}$$

and the normalized transition probability is given by

$$p_{ij}(k) = \frac{\tilde{p}_{ij}(k)}{\sum_{l=1}^{2} \tilde{p}_{il}(k)} \tag{39}$$

which ensures that $\sum_j p_{ij}(k) = 1$.

Common advantages include: ESKF generally exhibits higher precision under small-error conditions, while EKF tends to be more robust under highly nonlinear dynamics. By adaptively switching according to the estimated flight dynamics and filter consistency, the proposed IMF framework maintains stable estimation performance across different maneuvering conditions. In summary, the IMF framework effectively combines the strengths of EKF and ESKF, offering a more robust and flexible solution for GNSS/INS integrated navigation. The workflow of the IMF algorithm is shown in Figure 1.

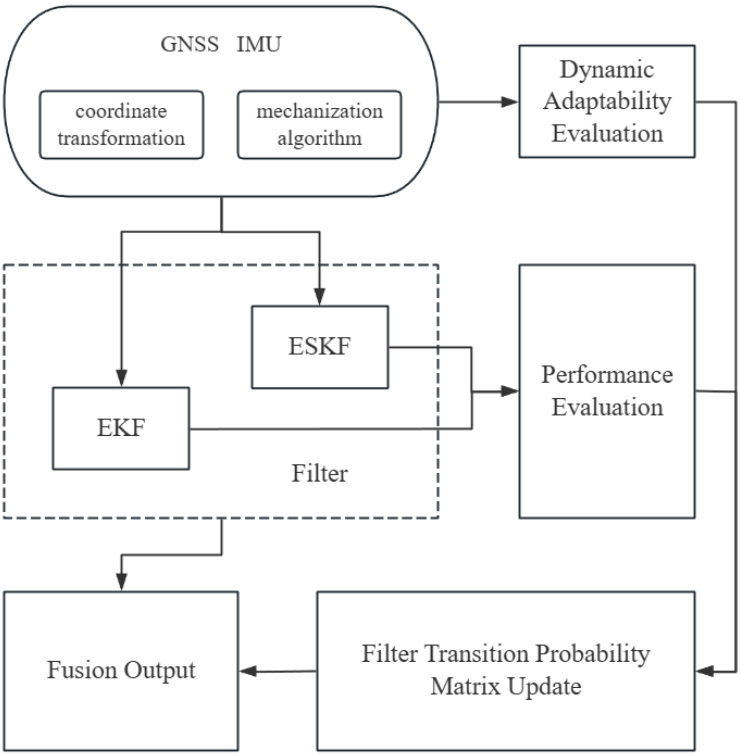


Figure 1. Interaction multi-filter framework.

4. Simulation and Analysis

Experimental data were sourced from an open-source GNSS/INS dataset provided by the Multi-Source Intelligent Navigation Laboratory at Wuhan University. The dataset, collected in an open industrial area, spans 3412 s (57 min) and comprises raw IMU measurements, GNSS positioning data, and ground-truth reference trajectories. GNSS and

IMU data were sampled at 1 Hz and 200 Hz, respectively. The inertial measurements were recorded using a MEMS IMU (ICM20602). According to the dataset specifications, the angle random walk and velocity random walk of the IMU are 0.2 deg $/\sqrt{\text{h}}$ and 0.2 m$/$s$/\sqrt{\text{h}}$, respectively, while the standard deviations of the gyroscope bias and accelerometer bias are 200 deg /h and 1000 mGal. For GNSS measurements, the dataset documentation specifies positioning standard deviations of 0.5, 0.5, and 0.8 m along the latitude, longitude, and height, respectively. As the specific GNSS receiver model is not explicitly provided in the dataset documentation, these reported positioning standard deviations were directly adopted to model the GNSS measurement noise in the navigation experiments. Based on the ground-truth reference trajectory, the speed ranges from 0 to 15.86 m/s, and the yaw rate varies between -25.91 and 22.55 deg/s, indicating the presence of both steady-motion and maneuvering segments. Figure 2 depicts the ground-truth trajectory in the north-east frame, originating from the starting point and concluding at the endpoint. The path forms a closed-loop rectangular pattern with multiple turns, spanning approximately 1200 m in the east direction and 1200 m in the north direction.

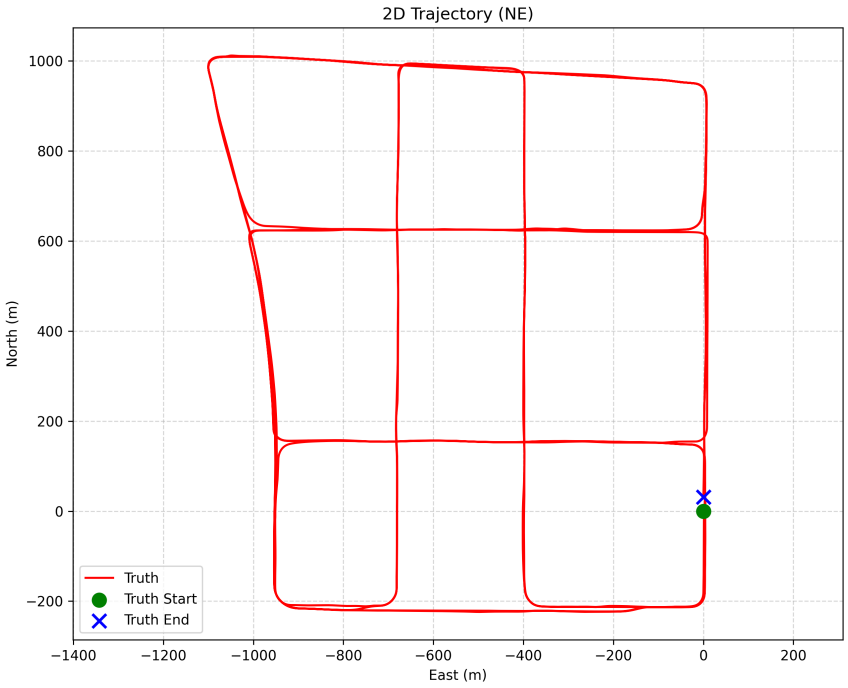


Figure 2. Ground truth 2D trajectory.

Navigation performance was evaluated by comparing position estimates in the north-east-down frame with ground truth under three configurations: standalone EKF, standalone ESKF, and the proposed IMF-based framework, which integrates EKF and ESKF.

Figure 3 illustrates position errors under the standalone EKF implementation. Significant deviations are observed, with root-mean-square errors of 0.684 m (north) and 0.716 m (east), indicating suboptimal positioning accuracy. The corresponding position errors using the standalone ESKF are shown below:

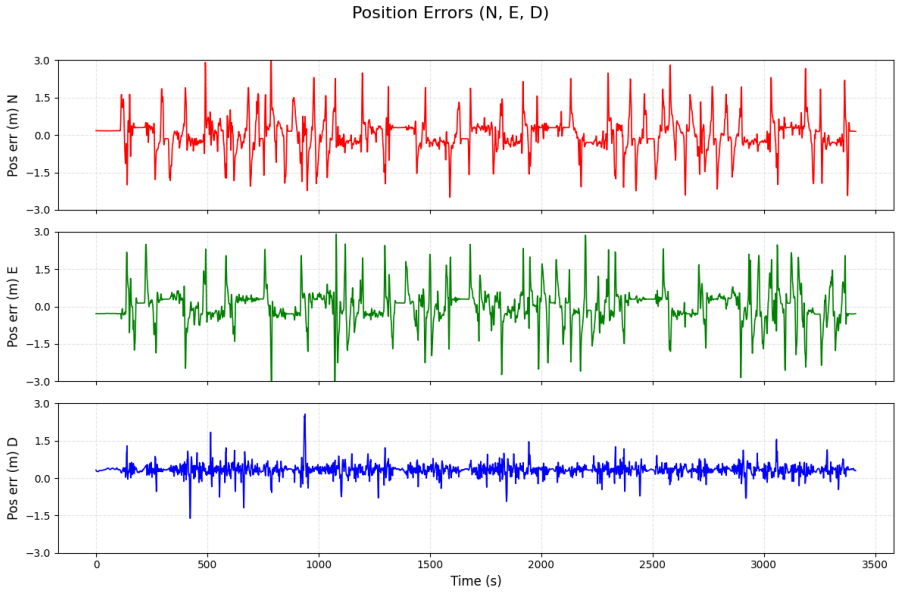


Figure 3. Position errors in the NED axes under EKF.

The ESKF-based navigation demonstrates moderate improvement, as shown in Figure 4, yielding RMSE values of 0.325 m (north) and 0.126 m (east). Although substantial initial errors arise during convergence, their magnitude diminishes as the estimation progresses. Figure 5 presents position errors under the IMF framework, with quantitative RMSE results summarized in Table 1. The IMF method exhibits markedly smoother and more stable error profiles across all NED axes compared to standalone filters. Position RMSE values are reduced to 0.142 m (north), 0.116 m (east), and 0.024 m (down), representing significant accuracy improvements.

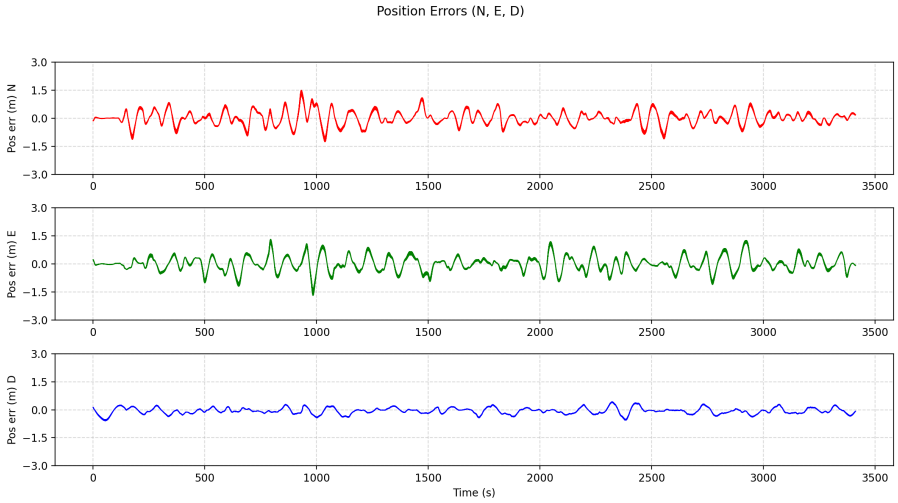


Figure 4. Position errors in the NED axes under ESKF.

In the final comparison, we evaluate the proposed IMF method against the AREKF method presented in reference [27]. The AREKF is a state-of-the-art integrated navigation algorithm built upon the interacting multiple model architecture. It addresses system uncertainties by fusing two distinct sub-models: an adaptive EKF that utilizes variational Bayesian inference to estimate time-varying process noise covariances online, and a robust EKF that employs K-means clustering to identify and mitigate measurement outliers. The AREKF was chosen because it represents an advanced solution that enhances navi-

gation reliability within a homogeneous filter structure. By comparing the proposed IMF framework with AREKF, this study aims to evaluate the effectiveness of the heterogeneous EKF/ESKF switching mechanism relative to representative adaptive EKF-based solutions. To ensure a fair comparison, the AREKF algorithm was re-implemented using the same dataset and measurement configurations as those adopted for the proposed method. As shown in Figure 6, the IMF method exhibits smaller and more stable errors across all directions. Specifically, in the north direction, the IMF method reduces the error by 14.46% compared to the AREKF method, and in the east direction, the improvement is even more pronounced, with a 29.70% reduction in error. These improvements indicate that the IMF method can effectively mitigate error accumulation and provide more reliable position estimates during dynamic scenarios.

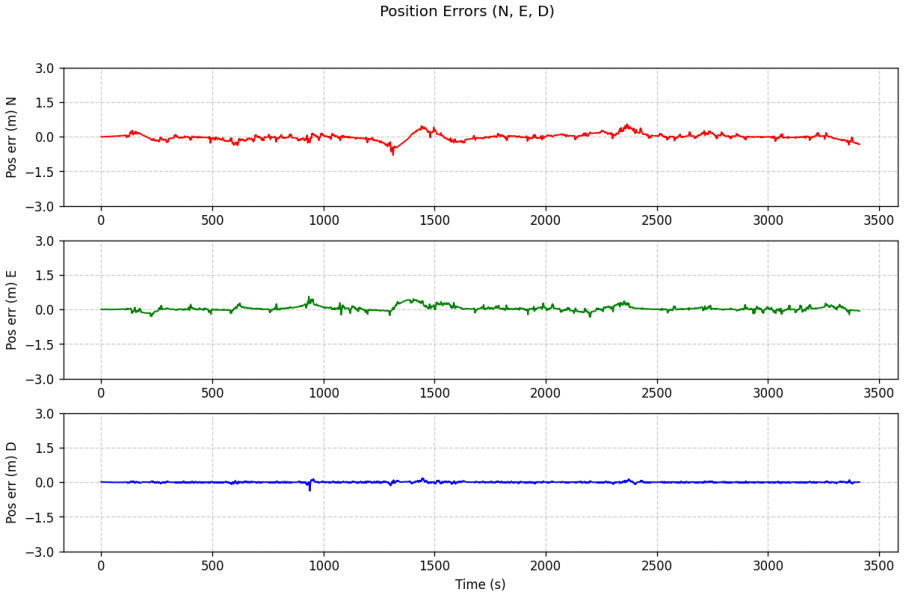


Figure 5. Position errors in the NED axes under IMF-based EKF/ESKF.

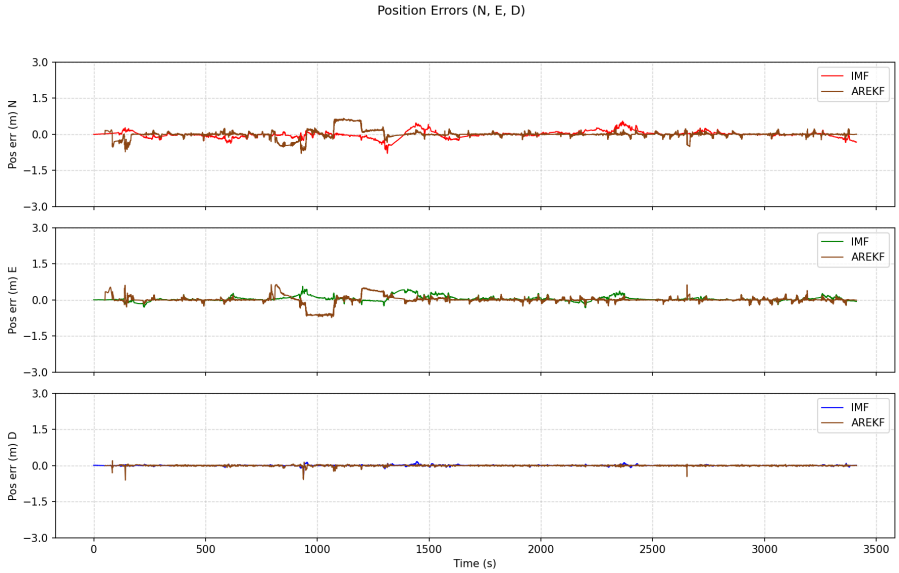


Figure 6. Position errors in the NED axes under IMF and AREKF.

The GNSS/INS combined navigation NED position errors under the different algorithms are illustrated as follows, along with the RMSE results summarized in a table:

Table 1. The RMSE and maximum error of navigation.

Position Error (m)	EKF	ESKF	AREKF	IMF
RMSE	0.581	0.250	0.136	0.107
RMSE (N)	0.684	0.325	0.166	0.142
RMSE (E)	0.716	0.126	0.165	0.116
RMSE (D)	0.184	0.256	0.029	0.024
MAX (N)	3.224	1.128	0.898	1.009
MAX (E)	3.272	0.376	0.734	0.567
MAX (D)	0.407	0.583	0.405	0.379

From the figures, it can be seen that the position error curves in the north, east, and down directions under the IMF method are smoother and more stable. The navigation results show clear improvements. The RMSE values for position in the three directions are 0.142 m, 0.116 m, and 0.024 m, respectively, all of which are smaller than those of the EKF and ESKF methods. These results indicate that the IMF algorithm effectively improves tracking accuracy. When using standalone filters, the error fluctuations are larger: under EKF, the position error in the east direction exceeds 3.272 m, whereas under ESKF it reaches 1.128 m. By contrast, the IMF-based GNSS/INS algorithm limits the navigation position error to within 1.009 m, and short-term errors remain constant regardless of the tracking duration.

As observed from the three-axis error plot, during the rapid, large-angle turns of the vehicle, reflecting the strongly nonlinear and non-stationary motion characteristics in this interval, all four methods exhibit varying degrees of fluctuations in the navigation results. Among them, the IMF method and AREKF method demonstrate the smallest fluctuations, with the IMF method generally maintaining a more stable performance. Notably, in the time interval from 1000 to 1500 s, the AREKF method exhibits more pronounced fluctuations than the IMF method. This difference can be attributed to the distinct decision-making mechanisms of the two approaches. AREKF operates within a homogeneous filtering structure and relies on adaptive noise estimation and robust statistical processing, whose effectiveness depends on the convergence of noise statistics and clustering results. During rapidly changing maneuvers, these adaptive processes may respond with a certain delay, leading to temporary performance degradation. In contrast, the proposed IMF framework employs a heterogeneous multi-filter architecture, in which EKF and ESKF run in parallel and are weighted through a joint decision mechanism based on residual likelihood and maneuver-dependent prior information. The maneuver intensity index provides an early indication of dynamic changes before significant residual growth occurs, enabling faster filter preference adjustment. As a result, IMF can more promptly reallocate filter weights and maintain stable estimation performance under high-dynamic conditions.

In summary, based on the simulation results, although the mean errors exhibit inevitable fluctuations during turning maneuvers, they remain smaller than those of standalone filters, and exhibit better navigation results than the AREKF method. Once turning is complete, the mean error oscillates around zero without divergence. The model validation shows that the IMF-based EKF/ESKF algorithm effectively improves filtering accuracy and enhances robustness against modeling errors and sensor uncertainties, achieves high navigation positioning precision, and enhances overall system robustness.

5. Conclusions

This study addresses filtering challenges in GNSS/INS integrated navigation systems, specifically targeting performance limitations inherent to single-filter architectures in diverse operational scenarios. We propose a novel interaction multi-filter framework that incorporates both EKF and ESKF and enables dynamic model selection. Building on the classical IMM methodology, the framework enables simultaneous parallel execution of the EKF and ESKF with probabilistic model updating. By real-time maneuver intensity

index and likelihood evaluation of each filter's performance, followed by dynamic model weighting and selection, this approach effectively mitigates the inherent constraints of standalone implementations while ensuring robust and stable navigation performance.

The simulation results demonstrate that the proposed IMF framework yields significant improvements in GNSS/INS integrated navigation accuracy over standalone EKF and ESKF implementations. The dataset trajectory features numerous large-angle right-angle turns, which more effectively showcases the enhanced reliability and robustness of the IMF architecture compared with single-filter approaches.Simulation analyses confirm that the proposed IMF framework significantly enhances the adaptability of navigation systems in complex environments. The IMF-based solution demonstrates superior positioning accuracy and robustness compared to independently implemented EKF and ESKF methodologies. The AREKF method significantly outperforms the EKF method, but its triaxial RMSE error and overall error are still higher than those of the IMF algorithm. Experimental validation establishes its capabilities in: (i) reducing estimation errors, (ii) suppressing INS sensor drift, and (iii) maintaining stability during nonlinear trajectories and high-dynamic maneuvers.

Future research will pursue two primary directions. First, it will extend the IMF framework to incorporate multi-sensor fusion (e.g., GNSS/INS/LiDAR/vision integration) to enhance positioning resilience in GNSS-denied environments. In parallel, implementation-oriented studies will be conducted to investigate real-time realization of the IMF framework on embedded onboard computing platforms for multirotor UAVs. These efforts will focus on evaluating real-time computational performance, filter switching behavior, and robustness under representative dynamic flight conditions, thereby facilitating practical deployment of the proposed approach in onboard GNSS/INS navigation systems. Second, integrating machine learning algorithms or adaptive statistical mechanisms to optimize the IMF transition probability matrix, thereby improving real-time adaptation to diverse operational conditions, will be pursued. These advancements will enable next-generation navigation systems with enhanced accuracy, greater robustness, and improved computational efficiency.

Author Contributions: S.Z.: Methodology, Software, Validation, Formal analysis, Data curation, Writing—Original Draft, Visualization. Z.Y.: Conceptualization, Supervision, Formal analysis, Writing—Review & Editing, Project administration, Funding acquisition. C.C.: Conceptualization, Supervision, Project administration, Funding acquisition, Writing—Review and Editing, Formal analysis. All authors have read and agreed to the published version of the manuscript.

Funding: The work is supported by the National Natural Science Foundation of China (Grant No: 62373192) and the Natural Science Foundation of Jiangsu Province (Grant No. BK20241484).

Data Availability Statement: The raw data supporting the conclusions of this article will be made available by the authors on request.

Acknowledgments: The authors are grateful to James Lam at HKU for insightful discussion.

Conflicts of Interest: The authors declare no competing conflicts of interest.

References

1. Gatkal, N.R.; Sachin, M.N.; Girishkumar, B.B.; Ramesh, K.S.; Avdhoot, A.W.; Pravin, B.K.; Ali, M. Review of UAVs for efficient agrochemical spray application. *Int. J. Agric. Biol. Eng.* **2025**, *18*, 1–9. [CrossRef]
2. Nex, F.; Armenakis, C.; Cramer, M.; Cucci, D.A.; Gerke, M.; Honkavaara, E.; Kukko, A.; Persello, C.; Skaloud, J. UAV in the advent of the twenties: Where we stand and what is next. *ISPRS J. Photogramm. Remote Sens.* **2022**, *184*, 215–242. [CrossRef]
3. Liu, C.; Nguyen, B.K. Low-Cost Real-Time Localisation for Agricultural Robots in Unstructured Farm Environments. *Machines* **2024**, *12*, 612. [CrossRef]
4. Yao, L.; Li, M.; Xu, T.; Dai, X.; Jiang, T.; Dai, P.; Wang, S.; Xing, J. GNSS/UWB/INS indoor and outdoor seamless positioning algorithm based on federal filtering. *Meas. Sci. Technol.* **2023**, *35*, 015135. [CrossRef]

5. Lin, H.Y.; Zhan, J.R. GNSS-denied UAV indoor navigation with UWB incorporated visual inertial odometry. *Measurement* **2023**, *206*, 112256. [CrossRef]
6. Chen, C.; Chang, G. Low-cost GNSS/INS integration for enhanced land vehicle performance. *Meas. Sci. Technol.* **2019**, *31*, 035009. [CrossRef]
7. Zhang, G.; Hsu, L.T. Intelligent GNSS/INS integrated navigation system for a commercial UAV flight control system. *Aerosp. Sci. Technol.* **2018**, *80*, 368–380. [CrossRef]
8. Causa, F.; Fasano, G.; Grassi, M. Improving autonomy in GNSS-challenging environments by multi-UAV cooperation. In Proceedings of the 2019 IEEE/AIAA 38th Digital Avionics Systems Conference (DASC), San Diego, CA, USA, 8–12 September 2019; pp. 1–10. [CrossRef]
9. Sivaneri, V.O.; Gross, J.N. Flight-testing of a cooperative UGV-to-UAV strategy for improved positioning in challenging GNSS environments. *Aerosp. Sci. Technol.* **2018**, *82*, 575–582. [CrossRef]
10. Fusini, L.; Fossen, T.I.; Johansen, T.A. Nonlinear observers for GNSS-and camera-aided inertial navigation of a fixed-wing UAV. *IEEE Trans. Control Syst. Technol.* **2017**, *26*, 1884–1891. [CrossRef]
11. Fan, Z.; Yang, P.; Mei, C.; Zhu, Q.; Luo, X. Fast attitude estimation system for unmanned ground vehicle based on vision/inertial fusion. *Machines* **2021**, *9*, 241. [CrossRef]
12. Liu, W.; Song, D.; Wang, Z.; Fang, K. Comparative Analysis between Error-State and Full-State Error Estimation for KF-Based IMU/GNSS Integration against IMU Faults. *Sensors* **2019**, *19*, 4912. [CrossRef] [PubMed]
13. Sahawneh, L.; Jarrah, M. Development and calibration of low cost MEMS IMU for UAV applications. In Proceedings of the 2008 5th International Symposium on Mechatronics and Its Applications, Amman, Jordan, 27–29 May 2008; pp. 1–9. [CrossRef]
14. Contreras, J.F.; Vassaram, J.A.; Fernandes, M.R.; do Val, J.B. Real-Time and Post-Mission Heading Alignment for Drone Navigation Based on Single-Antenna GNSS and MEMs-IMU Sensors. *Drones* **2025**, *9*, 169. [CrossRef]
15. Olesen, D.; Jakobsen, J.; Knudsen, P. Ultra-tightly coupled GNSS/INS for small UAVs. In Proceedings of the 30th International Technical Meeting of the Satellite Division of The Institute of Navigation (ION GNSS+ 2017), Portland, Oregon, 25–29 September 2017; pp. 2587–2602. [CrossRef]
16. Lee, J.; Kim, M.; Lee, J.; Pullen, S. Integrity assurance of Kalman-filter based GNSS/IMU integrated systems against IMU faults for UAV applications. In Proceedings of the 31st International Technical Meeting of the Satellite Division of The Institute of Navigation (ION GNSS+ 2018), Miami, FL, USA, 24–28 September 2018; pp. 2484–2500. [CrossRef]
17. Dorn, M.; Lesjak, R.; Wieser, M. Improvement of the standard GNSS/IMU solution for UAVs using already existing redundant navigation sensors. In Proceedings of the 2016 European Navigation Conference (ENC), Helsinki, Finland, 30 May–2 June 2016; pp. 1–9. [CrossRef]
18. Lei, B.; Liu, B.; Wang, C. Robust geometric control for a quadrotor UAV with extended Kalman filter estimation. *Actuators* **2024**, *13*, 205. [CrossRef]
19. Michalczyk, J.; Jung, R.; Weiss, S. Tightly-coupled ekf-based radar-inertial odometry. In Proceedings of the 2022 IEEE/RSJ International Conference on Intelligent Robots and Systems (IROS), Kyoto, Japan, 23–27 October 2022; pp. 12336–12343. [CrossRef]
20. Jing, X.; Cui, J.; He, H.; Zhang, B.; Ding, D.; Yang, Y. Attitude estimation for UAV using extended Kalman filter. In Proceedings of the 2017 29th Chinese Control and Decision Conference (CCDC), Chongqing, China, 28–30 May 2017; pp. 3307–3312. [CrossRef]
21. Kirubarajan, T.; Bar-Shalom, Y. Kalman filter versus IMM estimator: When do we need the latter? *IEEE Trans. Aerosp. Electron. Syst.* **2004**, *39*, 1452–1457. [CrossRef]
22. Ding, W.; Gao, Y. A quaternion based error state Kalman filter for attitude estimation using low-cost MEMS MARG sensors. In Proceedings of the 2020 IEEE 92nd Vehicular Technology Conference (VTC2020-Fall), Victoria, BC, Canada, 18 November–16 December 2020; pp. 1–5. [CrossRef]
23. Li, Z.; Zhang, Y. Constrained ESKF for UAV positioning in indoor corridor environment based on IMU and WiFi. *Sensors* **2022**, *22*, 391. [CrossRef] [PubMed]
24. Ren, Z.; Liu, S.; Dai, J.; Lv, Y.; Fan, Y. Research on Kinematic and Static Filtering of the ESKF Based on INS/GNSS/UWB. *Sensors* **2023**, *23*, 4735. [CrossRef] [PubMed]
25. Seah, C.E.; Hwang, I. Algorithm for performance analysis of the IMM algorithm. *IEEE Trans. Aerosp. Electron. Syst.* **2011**, *47*, 1114–1124. [CrossRef]
26. Yeom, S. Long distance moving vehicle tracking with a multirotor based on IMM-directional track association. *Appl. Sci.* **2021**, *11*, 11234. [CrossRef]
27. Zhao, C.; Chen, A.; Hua, L.; Lyu, Y.; Li, Y. An Adaptive Robust Filter for GNSS/INS Integrated Navigation System. In *Proceedings of the International Conference on Autonomous Unmanned Systems*; Springer: Singapore , 2023; pp. 118–128.

Disclaimer/Publisher's Note: The statements, opinions and data contained in all publications are solely those of the individual author(s) and contributor(s) and not of MDPI and/or the editor(s). MDPI and/or the editor(s) disclaim responsibility for any injury to people or property resulting from any ideas, methods, instructions or products referred to in the content.